

Computational calibration method for optical tomography

Tanja Tarvainen, Ville Kolehmainen, Marko Vauhkonen, Antti Vanne, Adam P. Gibson, Martin Schweiger, Simon R. Arridge, and Jari P. Kaipio

We propose a computational calibration method for optical tomography. The model of the calibration scheme is based on the rotation symmetry of source and detector positions in the measurement setup. The relative amplitude losses and phase shifts at the optic fibers are modeled by complex-valued coupling coefficients. The coupling coefficients can be estimated when optical tomography data from a homogeneous and isotropic object are given. Once these coupling coefficients have been estimated, any data measured with the same measurement setup can be corrected for the relative variation in the data due to source and detector losses. The final calibration of the data for the source and detector losses and the source calibration between the data and the forward model are obtained as part of the initial estimation for reconstruction. The calibration method was tested with simulations and measurements. The results show that the coupling coefficients of the sources and detectors can be estimated with good accuracy. Furthermore, the results show that the method can significantly improve the quality of reconstructed images. © 2005 Optical Society of America

OCIS codes: 100.3190, 170.5280, 170.6960.

1. Introduction

Diffuse optical tomography (DOT) is an imaging method that has potential applications in medical imaging, such as in detection of tumors from breast tissue and in monitoring of infant brain tissue oxygenation level and functional brain activation studies.^{1–7} In addition, there has been growing interest toward the use of optical methods in industrial process tomography.⁸ In DOT measurement, near-infrared laser light is guided into the object via source fibers and the intensity of transmitted light is measured with optic fibers and light-sensitive detectors on the boundary of the object. Based on the measurements, absorption and scattering coefficients within

the object are reconstructed. The image reconstruction in DOT is an ill-posed inverse problem, and thus the solution is very sensitive to measurement and modeling errors.

Among the key difficulties in DOT are the unknown amplitude losses and phase delays that are caused by the optic fibers and the coupling effects between the object and the optic fibers. Unless these losses are efficiently calibrated or modeled, they can result in severe artifacts in the reconstructed images. Typically, the errors in optode modeling appear as absorption and scattering perturbations adjacent to the optodes.

One way to compensate for the optode losses is to use difference imaging. Difference imaging is known to produce images with few artifacts. However, it cannot be used when absolute baseline optical properties are required or when a reference measurement is not available.⁹ Therefore, to obtain absolute images, an efficient calibration protocol is needed.

Methods for calibration of source and detector optode losses by use of calibration tools or other instrumentation-based methods have been described (for example, in Refs. 10–12). However, the accurate calibration of source and detector losses is difficult to implement on the instrumentation level. Therefore other model-based methods have been developed. A method in which the amplitude losses were solved as

T. Tarvainen (Tanja.Tarvainen@uku.fi), V. Kolehmainen, M. Vauhkonen, A. Vanne, and J. P. Kaipio are with the Department of Applied Physics, University of Kuopio, P.O. Box 1627, FIN-70211 Kuopio, Finland. A. P. Gibson is with the Department of Medical Physics and Bioengineering, University College London, 11-20 Copper Street, London, WC1E 6JA, United Kingdom. M. Schweiger and S. R. Arridge are with the Department of Computer Science, University College London, Gower Street, London, WC1E 6BT, United Kingdom.

Received 15 June 2004; revised manuscript received 19 November 2004; accepted 19 November 2004.

0003-6935/05/101879-10\$15.00/0

© 2005 Optical Society of America

part of the reconstruction problem was introduced in Ref. 13. The method was further extended to correct small errors in optode positions¹⁴ and phase delays.¹⁵ The simultaneous image reconstruction and optode calibration is an efficient way to compensate for optode losses, but the method does not ensure absolute calibration and is computationally demanding. Furthermore, the method may partially explain information in the data by the optode losses, leading to blurring of reconstructed targets that locate in the proximity of the optodes. Another approach described in Ref. 16 uses homogeneous phantom measurements for calibration. The estimation of the optode losses is based on minimization of the least-squares error between the homogeneous phantom data and the diffusion approximation (DA) model. The method is practical, and the same algorithm can be used to estimate the initial optical properties for reconstructions. However, owing to the nature of the problem, the calibration procedure is sensitive to the initial guess of the phantom optical properties.

In this paper we propose a novel computational method for calibration of diffuse optical tomography measurements. The model of the calibration scheme is based on the rotation symmetry of source and detector positions in the measurement setup. Rotation symmetric measurement setups are typically used in many applications of DOT, such as when a cylindrical measurement cell is used. In the calibration model, the relative amplitude losses and phase shifts in the optic fibers are modeled by complex-valued coupling coefficients. A similar type of model for the calibration of continuous-wave measurements was presented previously in Ref. 17. Here a model for frequency-domain data is given, and the calibration procedure is somewhat different from the method used in Ref. 17. In the proposed approach, the source and detector coupling coefficients are estimated by use of the data of homogeneous and isotropic material. Because of the simple calibration model, the estimation of the coupling coefficients is well posed. Furthermore, prior information about the optical properties of the calibration material and the strength of the light source is not needed in the estimation of the coupling coefficients. These facts make the estimation procedure simple, fast, and accurate.

Once these coupling coefficients have been estimated from the calibration data, any data measured with the same measurement setup can be corrected for the relative variations in the data that are due to the amplitude losses and phase shifts in the optic fibers. That is, the coupling coefficients do not need to be redefined as long as the measurement setup remains unchanged. Finally, the final calibration of the data for the source and detector losses and the source calibration between the data and the forward model are obtained as part of the initial estimation for reconstruction.

The paper is organized as follows. In Section 2 the calibration model is formulated and the estimation of the coupling coefficients is defined as a minimization problem. Then the calibration of the data by the es-

timated coefficients and the initial estimation for reconstruction are discussed. In Section 3 a finite-element model (FEM) for the DA that includes the source and detector coupling coefficients is introduced. In Section 4 the results of the simulations and measurements are shown. In Section 5 conclusions are given.

2. Methods

A. Calibration Model

Let $\Omega \subset \mathbb{R}^n$, $n = 2$ or 3 be a circular, cylindrical, or spherical domain with boundary $\partial\Omega$. The medium Ω is assumed to be homogeneous and isotropic, i.e., the absorption and scattering coefficients are assumed to be constant within the medium, and the scattering phase is assumed to depend only on the angle between incoming and outgoing directions. Furthermore, let m sources and m detectors be placed in circular symmetrical positions on the boundary of the domain. We note that the number of the sources and the number of detectors do not need to be identical. However, we use that assumption here to simplify the notations. Furthermore, in most applications of DOT the number of the sources and detectors is the same. In the sequel, the locations of the sources are denoted by ε_i , $i = 1, \dots, m$, and the locations of the detectors are denoted by ζ_i , $i = 1, \dots, m$.

Let us first assume that all sources and detectors are ideal in the sense that no amplitude losses or phase delays occur in the source and detector fibers. If light is guided into the object via sources at $\varepsilon_1, \dots, \varepsilon_m$ and is measured by detectors at ζ_1, \dots, ζ_m each time in that order, the measured frequency-domain data can be written in the form

$$\begin{aligned} Z &= \begin{pmatrix} z_{1,1} & z_{2,1} & \dots & z_{m,1} \\ z_{1,2} & z_{2,2} & & z_{m,2} \\ \vdots & & & \vdots \\ z_{1,m} & z_{2,m} & \dots & z_{m,m} \end{pmatrix} \\ &= \begin{pmatrix} y_1 \exp(j\eta_1) & y_m \exp(j\eta_m) & \dots & y_2 \exp(j\eta_2) \\ y_2 \exp(j\eta_2) & y_1 \exp(j\eta_1) & & y_3 \exp(j\eta_3) \\ \vdots & \vdots & & \vdots \\ y_m \exp(j\eta_m) & y_{m-1} \exp(j\eta_{m-1}) & \dots & y_1 \exp(j\eta_1) \end{pmatrix}, \end{aligned} \quad (1)$$

where $z_{i,k}$ denotes the measurement for source i and detector k . Thus, in the rotation symmetric setup, the measured amplitudes and phases are, in the ideal case, equal when the angle between the source and the detector is equal. In the sequel we denote this ideal rotation symmetric measurement vector by

$$\hat{y} = (y_1 \exp(j\eta_1), \dots, y_m \exp(j\eta_m))^T, \quad (2)$$

where j is the imaginary unit, y_i is the amplitude, and η_i is the phase shift of the transmitted light with a source–detector angle index i .

In real measurements, an unknown amount of am-

plitude loss and phase delay is caused by the source and the detector fibers and by the coupling effects between the object and the optic fibers. Next we model these unknown losses by using complex-valued coupling coefficients. We write the model as

$$x_{i,k} = \hat{s}_i \hat{d}_k z_{i,k} = s_i \exp(j\sigma_i) d_k \exp(j\delta_k) z_{i,k}, \quad (3)$$

where $x_{i,k}$ is the measured intensity for the source–detector pair (i, k) , \hat{s}_i is the coupling coefficient of the source (s_i is the source amplitude loss coefficient; σ_i is the source phase shift), \hat{d}_k is the coupling coefficient of the detector (d_k is the detector amplitude loss coefficient; δ_k is the detector phase shift), and $z_{i,k}$ is the ideal measured intensity as in Eq. (1).

Consider next the implementation of the model for the calibration data. In typical DOT, measurement light is guided into the object via one of the source fibers at $\varepsilon_1, \dots, \varepsilon_m$, and the intensity of the transmitted light is measured by the detectors at ζ_1, \dots, ζ_m . Let us concatenate the source coupling coefficients to a vector $\hat{s} = [s_1 \exp(j\sigma_1), \dots, s_m \exp(j\sigma_m)]^T$, where $s = (s_1, \dots, s_m)^T$ is the source amplitude loss coefficient and $\sigma = (\sigma_1, \dots, \sigma_m)^T$ is the source phase shift. Similarly, let us concatenate the detector coupling coefficients to a vector $\hat{d} = [d_1 \exp(j\delta_1), \dots, d_m \exp(j\delta_m)]^T$, where $d = (d_1, \dots, d_m)^T$ is the detector amplitude loss coefficient and $\delta = (\delta_1, \dots, \delta_m)^T$ is the detector phase shift. Exploiting the rotation symmetry of the ideal measurement \hat{y} , in Eq. (2), the model for the calibration data can be written in the form

$$\begin{aligned} X &= \begin{bmatrix} x_{1,1} & \dots & x_{m,1} \\ \vdots & \ddots & \vdots \\ x_{1,m} & \dots & x_{m,m} \end{bmatrix} \\ &= \begin{bmatrix} d_1 \exp(j\delta_1) & & & \\ & \ddots & & \\ & & d_m \exp(j\delta_m) & \\ y_1 \exp(j\eta_1) & \dots & y_2 \exp(j\eta_2) & \\ \vdots & \ddots & \vdots & \\ y_m \exp(j\eta_m) & \dots & y_1 \exp(j\eta_1) & \\ s_1 \exp(j\sigma_1) & & & \\ & \ddots & & \\ & & s_m \exp(j\sigma_m) & \end{bmatrix} \\ &= DYS, \end{aligned} \quad (4)$$

where D and S are diagonal matrices that contain the detector and source coupling coefficients and Y is a matrix that contains the ideal measurements.

B. Estimation of the Optode Coupling Coefficients

Given the model [Eq. (4)], the calibration problem is to estimate the unknown amplitude loss coefficients $(s_1, \dots, s_m)^T$ and $(d_1, \dots, d_m)^T$ and phase shifts $(\sigma_1, \dots, \sigma_m)^T$ and $(\delta_1, \dots, \delta_m)^T$ that occur in the source and detector fibers, as well as the amplitudes

$(y_1, \dots, y_m)^T$ and the phase shifts $(\eta_1, \dots, \eta_m)^T$ of the transmitted light when measured data from a homogeneous and isotropic object are given.

The problem is nonunique, and therefore all calibration parameters describing amplitude losses and phase shifts cannot be solved. To overcome the non-uniqueness problem, we form relative parameters as follows. We choose the coupling coefficients of the first source and the first detector as references and define the relative amplitude loss coefficients, \tilde{s}_i and \tilde{d}_i , and the relative amplitudes \tilde{y}_i of the transmitted light as

$$\tilde{s}_i = s_i/s_1, \quad i = 1, \dots, m, \quad (5)$$

$$\tilde{d}_i = d_i/d_1, \quad i = 1, \dots, m, \quad (6)$$

$$\tilde{y}_i = y_i s_1 d_1, \quad i = 1, \dots, m. \quad (7)$$

Similarly, we define relative phase shifts, $\tilde{\sigma}_i$ and $\tilde{\delta}_i$, and relative phase shifts $\tilde{\eta}_i$ of the transmitted light as

$$\tilde{\sigma}_i = \sigma_i - \sigma_1, \quad i = 1, \dots, m, \quad (8)$$

$$\tilde{\delta}_i = \delta_i - \delta_1, \quad i = 1, \dots, m, \quad (9)$$

$$\tilde{\eta}_i = \eta_i + \sigma_1 + \delta_1, \quad i = 1, \dots, m. \quad (10)$$

Now, based on the definitions in Eqs. (5)–(10), the relative amplitude loss coefficient and phase shift of the first source are $\tilde{s}_1 = 1$ and $\tilde{\sigma}_1 = 0$, respectively. Similarly, the relative amplitude loss coefficient and phase shift of the first detector are $\tilde{d}_1 = 1$ and $\tilde{\delta}_1 = 0$, respectively. Using the relative parameters defined in Eqs. (5)–(10), the data in Eq. (4) can be written in the form

$$\begin{aligned} X &= \begin{bmatrix} 1 & & & \\ \tilde{d}_2 \exp(j\tilde{\delta}_2) & & & \\ & \ddots & & \\ & & \tilde{d}_m \exp(j\tilde{\delta}_m) & \\ \tilde{y}_1 \exp(j\tilde{\eta}_1) & \dots & \tilde{y}_2 \exp(j\tilde{\eta}_2) & \\ \tilde{y}_2 \exp(j\tilde{\eta}_2) & \ddots & \tilde{y}_3 \exp(j\tilde{\eta}_3) & \\ \vdots & \ddots & \vdots & \\ \tilde{y}_m \exp(j\tilde{\eta}_m) & \dots & \tilde{y}_1 \exp(j\tilde{\eta}_1) & \\ 1 & & & \\ \tilde{s}_2 \exp(j\tilde{\eta}_2) & & & \\ & \ddots & & \\ & & \tilde{s}_m \exp(j\tilde{\eta}_m) & \end{bmatrix} \\ &= \tilde{D} \tilde{Y} \tilde{S}. \end{aligned} \quad (11)$$

The calibration problem is now to estimate the relative source and detector amplitude-loss coefficients $(\tilde{s}_2, \dots, \tilde{s}_m)^T$ and $(\tilde{d}_2, \dots, \tilde{d}_m)^T$, respectively, the relative source and detector phase shifts $(\tilde{\sigma}_2, \dots, \tilde{\sigma}_m)^T$ and $(\tilde{\delta}_2, \dots, \tilde{\delta}_m)^T$, respectively; the relative ampli-

tudes $(\tilde{y}_1, \dots, \tilde{y}_m)^T$; and the relative phase shifts $(\tilde{\eta}_1, \dots, \tilde{\eta}_m)^T$ of the transmitted light when the measured data from a homogeneous and isotropic object are given. The relative amplitude-loss and phase-shift parameters can be estimated in the least-squares sense by minimization of the following functional:

$$\Psi = \left\| L \left\{ \begin{bmatrix} |\Gamma_0| \\ \text{ang}(\Gamma_0) \end{bmatrix} - \begin{bmatrix} |X(\tilde{y}, \tilde{s}, \tilde{d})| \\ \text{ang}(X(\tilde{\eta}, \tilde{\sigma}, \tilde{\delta})) \end{bmatrix} \right\} \right\|_2^2, \quad (12)$$

where $|\Gamma_0|$ and $\text{ang}(\Gamma_0)$ contain the amplitudes and phase shifts of the calibration data in vector form, respectively, and $|X(\tilde{y}, \tilde{s}, \tilde{d})|$ and $X(\tilde{\eta}, \tilde{\sigma}, \tilde{\delta})$ are the amplitude and phase-shift vectors, respectively, that are obtained from the solution of the model [Eq. (11)]. The matrix L is a weight matrix that basically corresponds to the Cholesky factor of the inverse of the noise covariance matrix. In DOT, where the dynamic range of the measured light intensities is often quite large, scaling of the data may be needed to ensure numerical stability of the optimization algorithm. In such cases, the weight matrix is often chosen as a diagonal matrix:

$$L = \text{diag} \left[\begin{bmatrix} |\Gamma_0| \\ \text{ang}(\Gamma_0) \end{bmatrix} \right]^{-1}. \quad (13)$$

The minimization of Eq. (12) can be solved, for example, with the Gauss–Newton method, which can be written in the form

$$\theta_{i+1} = \theta_i + c_i (J_i^T W J_i)^{-1} J_i^T W \left\{ \begin{bmatrix} |\Gamma_0| \\ \text{ang}(\Gamma_0) \end{bmatrix} - \begin{bmatrix} |X(\theta_i)| \\ \text{ang}(X(\theta_i)) \end{bmatrix} \right\}, \quad (14)$$

where

$$\theta = (\tilde{y}_1, \dots, \tilde{y}_m, \tilde{s}_2, \dots, \tilde{s}_m, \tilde{d}_2, \dots, \tilde{d}_m, \tilde{\eta}_1, \dots, \tilde{\eta}_m, \tilde{\sigma}_2, \dots, \tilde{\sigma}_m, \tilde{\delta}_2, \dots, \tilde{\delta}_m)^T \in \mathbb{R}^{6m-4}$$

is the vector of unknown parameters, $X(\theta_i)$ implements the calibration model [Eq. (11)] in vector form, c_i is a step-length parameter, $W = L^T L$, and matrix J_i is the Jacobian for $|X(\theta_i)|$ and $\text{ang}(X(\theta_i))$.

In some cases data cannot be measured from all the detectors because of too large a dynamic range of the light intensities, and thus the coupling coefficient estimation problem may become ill posed. In such cases, one possibility is to solve Eq. (12) by use of the Levenberg–Marquardt algorithm, which can be written in the form

$$\theta_{i+1} = \theta_i + c_i (J_i^T W J_i + \lambda I)^{-1} J_i^T W \left\{ \begin{bmatrix} |\Gamma_0| \\ \text{ang}(\Gamma_0) \end{bmatrix} - \begin{bmatrix} |X(\theta_i)| \\ \text{ang}(X(\theta_i)) \end{bmatrix} \right\}, \quad (15)$$

where λ is a Levenberg–Marquardt stabilization parameter and I is an identity matrix.¹⁸

C. Calibration

Once the relative source and detector amplitude-losses and phase shifts have been estimated, any data that have been measured with the same measurement setup can be calibrated for the relative variations in the data owing to the source and detector losses. The calibration of the measurement data is based on Eq. (11), and it is obtained by dividing the measured data Γ by the estimated relative source and detector coupling coefficients. Assuming that the data Γ is arranged in matrix form as in Eq. (11), the calibrated data $\tilde{\Gamma}$ is obtained by

$$\tilde{\Gamma} = \tilde{D}^{-1} \Gamma \tilde{S}^{-1}, \quad (16)$$

where \tilde{D} is a diagonal matrix that contains the estimated relative detector coupling coefficients $\tilde{d}_i \exp(j\tilde{\delta}_i)$ and \tilde{S} is a diagonal matrix that contains the estimated relative source coupling coefficients $\tilde{s}_k \exp(j\tilde{\delta}_k)$.

It should be noted that calibration Eq. (16) corrects the data only for the relative variations in the amplitude losses and phase shifts in the detector and source fibers. The calibrated data $\tilde{\Gamma}$ in Eq. (16) contain a constant multiplicative bias in amplitude and a constant additive bias in phase that are due to use of the relative amplitude loss and phase-shift parameters in the estimation. Basically, the magnitude of these biases is defined by the unknown amplitude loss and phase-shift coefficients of the first source and detector. Formally, the magnitude of the multiplicative bias in the amplitude of the data $\tilde{\Gamma}$ would be $\xi = s_1 d_1$, and the magnitude of the additive bias in phase would be $\varepsilon = \sigma_1 + \delta_1$ [see Eqs. (7) and (10)]. These biases have to be estimated and removed from the calibrated data $\tilde{\Gamma}$ before reconstruction. This is explained in the next section.

D. Initialization for Reconstruction

Owing to the ill-posed nature of the DOT problem, the initial values of the optical properties for the image reconstruction algorithm need to be reasonably close to the actual (heterogeneous) optical properties to guarantee fast convergence in image reconstruction. One possible solution for the initialization is to initialize the absorption and scatter images to global parameter values $(\mu_{a,0}, \mu'_{s,0}) \in \mathbb{R}^2$ that are obtained as a minimizer of the least-squares error between the measured and the computed data. Here we discuss how the constant biases in the amplitude and phase of the calibrated data $\tilde{\Gamma}$ can be estimated as part of the minimization problem.

Let

$$|\Gamma| = F_{\text{mod}}(\mu_a, \mu'_s), \quad (17)$$

$$\text{ang}(\Gamma) = F_{\text{ang}}(\mu_a, \mu'_s), \quad (18)$$

denote the forward models that map the absorption and scatter parameters $(\mu_{a,0}, \mu'_{s,0})$ to the vectors of amplitude and phase-shift data. In this study the forward models [Eqs. (17) and (18)] are based on the DA.

The calibrated data in Eq. (16) contain unknown bias, which is due to use of the relative detector and source amplitude loss and phase-shift coefficients in the calibration. The amplitude data contain a multiplicative bias, and thus we write the model

$$|\tilde{\Gamma}| = G_{\text{mod}}(\mu_a, \mu'_s, \xi) = \xi F_{\text{mod}}(\mu_a, \mu'_s), \quad (19)$$

where the scalar parameter ξ is the bias variable. The bias in the phase data is additive, and thus we write the model

$$\text{ang}(\tilde{\Gamma}) = G_{\text{ang}}(\mu_a, \mu'_s, \varepsilon) = F_{\text{ang}}(\mu_a, \mu'_s) + \varepsilon, \quad (20)$$

where the scalar ε denotes the bias in phase.

Using the models [Eqs. (19) and (20)], the initial estimation is defined as finding the parameter vector $(\mu_{a,0}, \mu'_{s,0}, \xi, \varepsilon)^T \in \mathbb{R}^4$ that minimizes the functional

$$\Psi = \left\| L \left\{ \begin{bmatrix} |\tilde{\Gamma}| \\ \text{ang}(\tilde{\Gamma}) \end{bmatrix} - \begin{bmatrix} G_{\text{mod}}(\mu_{a,0}, \mu'_{s,0}, \xi) \\ G_{\text{ang}}(\mu_{a,0}, \mu'_{s,0}, \varepsilon) \end{bmatrix} \right\} \right\|_2^2, \quad (21)$$

where vectors $|\tilde{\Gamma}|$ and $\text{ang}(\tilde{\Gamma})$ contain the amplitudes and phase shifts of the calibrated data, respectively. Once Eq. (21) is solved, one can remove the estimated bias (ξ, ε) from the calibrated data by

$$|\tilde{\Gamma}| = \xi^{-1} |\tilde{\Gamma}|, \quad \text{ang}(\tilde{\Gamma}) = \text{ang}(\tilde{\Gamma}) - \varepsilon \quad (22)$$

and compute the reconstructions in the conventional way, using the forward models [Eqs. (17) and (18)] and the estimated $(\mu_{a,0}, \mu'_{s,0})$ as the starting point in the reconstruction algorithm.

Note that often in practical DOT experiments, the calibration of the source model in the forward model (e.g., DA) with respect to the strength and initial phase of the light source in the experimental device is not known. However, these unknowns are naturally embedded in the values of the parameters (ξ, ε) as $\xi = s_1 d_1 I$ and $\varepsilon = \sigma_1 + \delta_1 + \theta$, where I and θ denote the strength and initial phase of the light source, respectively. Thus Eq. (22) also calibrates the data $\tilde{\Gamma}$ with respect to the source model.

3. Extended Diffusion Approximation Model for Diffuse Optical Tomography

The source and detector coupling coefficients can also be included in the DA model for optical tomography measurements. In this section the extended model, which includes the source and detector coupling coefficients, and the FE discretization of the model are discussed. The model is used to generate data for the simulations presented in Section 4.

A. Extended Diffusion Approximation Model

The frequency-domain version of the DA assumes the form¹⁹

$$-\nabla \cdot \kappa \nabla \Phi(r; \omega) + \mu_a \Phi(r; \omega) + (j\omega/c) \Phi(r; \omega) = q_0(r; \omega), \quad (23)$$

where $\Phi(r; \omega) =: \Phi(r)$ is the photon density, κ is the diffusion coefficient, μ_a is the absorption coefficient, j is the imaginary unit, ω is the angular modulation frequency of the input signal, c is the speed of light in the medium, and $q_0(r; \omega) =: q_0(r)$ is the source within Ω . The diffusion coefficient κ is of the form²⁰

$$\kappa = \frac{1}{n(\mu_a + \mu'_s)}, \quad (24)$$

where n is the dimension of the domain ($=2, 3$) and μ'_s is the reduced scattering coefficient. The Robin-type boundary condition for the DA can be derived to have the form

$$\Phi(r) + \frac{1}{2\gamma_n} \kappa A \frac{\partial \Phi(r)}{\partial \hat{n}} = 0, \quad r \in \partial\Omega, \quad (25)$$

where γ_n is a dimension-dependent constant, which obtains values $\gamma_2 = 1/\pi$ and $\gamma_3 = 1/4$, and A is a parameter governing the internal reflection at the boundary $\partial\Omega$.²⁰

The light sources at $\partial\Omega$ are usually modeled in the DA either by the collimated source model or by the diffuse boundary source model. In the case of the collimated source model, the collimated light source is modeled as an isotropic point source located at a depth $(1/\mu'_s)$ below the source site at $\partial\Omega$.²¹ Including the source coupling coefficient, the collimated source model assumes the form

$$q_0(r) = \hat{s}_i \delta(r - r_s), \quad (26)$$

where the position r_s is located at a depth $(1/\mu'_s)$ below the source site and $\hat{s}_i = s_i \exp(j\sigma_i)$ is the coupling coefficient at source site ε_i , as described in Section 2. In the case of the diffuse boundary source model, the source is modeled as an inward-directed diffuse boundary current at the source site ε_i .²¹ The boundary condition in Eq. (25) with the diffuse source model, including the source coupling coefficient \hat{s}_i , can be written as

$$\Phi(r) + \frac{1}{2\gamma_n} \kappa A \frac{\partial \Phi(r)}{\partial \hat{n}} = \begin{cases} -\frac{\hat{s}_i w_i}{\gamma_n} & r \in \cup_i \varepsilon_i \\ 0 & r \in \partial \Omega \setminus \cup_i \varepsilon_i \end{cases}, \quad (27)$$

$$\tilde{G} = 0, \quad (34)$$

where the indicator function w_i for the source site ε_i is either 1 or 0, depending on whether the source is on.

The measured quantity, which is the exitance $\Gamma(r)$, is explained, for example, in Refs. 22 and 20. Including the detector coupling coefficient, the measured quantity can be written in the form

$$\Gamma(r) = -\hat{d}_i \kappa \frac{\partial \Phi(r)}{\partial \hat{n}} = \hat{d}_i \frac{2\gamma_n}{A} \Phi(r), \quad r \in \cup_i \zeta_i, \quad (28)$$

where $\hat{d}_i = d_i \exp(j\delta_i)$ is the coupling coefficient of the detector at ζ_i , as described earlier in Section 2.

B. Finite-Element Discretization

The FE approximation of the DA has been derived previously (e.g., in Refs. 23 and 20). Here the FE approximation for the extended DA is constructed similarly to the FE approximation for the DA in Ref. 24.

Accordingly, the solution $\Phi(r)$ of the variational formulation of Eq. (23) is approximated in a piecewise linear basis $\Phi^h = \sum_{k=1}^N a_k \varphi_k$, where φ_k are nodal basis functions of the FE mesh and a_k are photon densities in the nodal points of the FE mesh. The FE approximation of the extended DA can be written as

$$(K + C + R + j\omega Z)a = \tilde{G} + \tilde{E}, \quad (29)$$

where

$$K(p, k) = \int_{\Omega} \kappa \nabla \varphi_k \cdot \nabla \varphi_p \, dr, \quad (30)$$

$$C(p, k) = \int_{\Omega} \mu_a \varphi_k \varphi_p \, dr, \quad (31)$$

$$Z(p, k) = \frac{1}{c} \int_{\Omega} \varphi_k \varphi_p \, dr, \quad (32)$$

$$R(p, k) = \int_{\partial \Omega} \frac{2\gamma_n}{A} \varphi_k \varphi_p \, dS, \quad (33)$$

where $k, p = 1, \dots, N$. The source vector on the right-hand side of Eq. (29) depends on the source model that is used. In the case of the collimated source model [Eq. (26)], the source vectors \tilde{G} and \tilde{E} are of the form

$$\tilde{E}(p) = s_i \exp(j\sigma_i) \int_{\Omega} \delta(r - r_s) \varphi_p \, dr, \quad (35)$$

where s_i is the source amplitude loss coefficient and σ_i is the source phase shift. In the case of a diffuse boundary source model, the source vectors are of the form

$$\tilde{G}(p) = s_i \exp(j\sigma_i) \int_{\partial \Omega} \frac{-2w_i}{A} \varphi_p \, dS, \quad (36)$$

$$\tilde{E} = 0. \quad (37)$$

The exitance Γ at the source site is obtained by

$$\Gamma = Ma, \quad (38)$$

where M is a matrix of the form

$$M(i, k) = \begin{cases} [2d_i \exp(j\delta_i) \gamma_n / A] & \text{if node } k \in \zeta_i \subset \partial \Omega \\ 0 & \text{otherwise} \end{cases}, \quad (39)$$

where $k = 1, \dots, N$; $i = 1, \dots, m$; d_i is the detector amplitude loss coefficient; and δ_i is the detector phase shift.

4. Results

The calibration method was tested with simulations and measurements. The purpose of the simulations was to test the validity of the source and detector coupling coefficient estimation method and to inspect the effect of the calibration on the data and the reconstructed images. Then the effects of the calibration on the measured data and the quality of the reconstructed images were investigated.

A. Simulation Results

In the simulations, the two-dimensional ($n = 2$) case was considered. The medium $\Omega \subset \mathbb{R}^2$ was a circular domain with diameter $d = 5$ cm. Sixteen equally spaced sources and 16 equally spaced detectors were located on the boundary of the domain. The absorption coefficient and the (reduced) scattering coefficient were chosen as $\mu_a = 0.025 \text{ mm}^{-1}$ and $\mu'_s = 2 \text{ mm}^{-1}$, respectively. The modulation frequency of the input signal was $f = 100$ MHz. The source and detector amplitude loss coefficients were generated randomly from uniform distribution $[0.75, 1]$, and the source and detector phase shifts were generated randomly from uniform distribution $[-\pi/120, 0]$. The data were generated with the FE model for the extended DA with the collimated source model [see Eqs. (29), (35), and (38)]. The FE mesh contained 58,238 triangular elements and 30,704 nodal points.

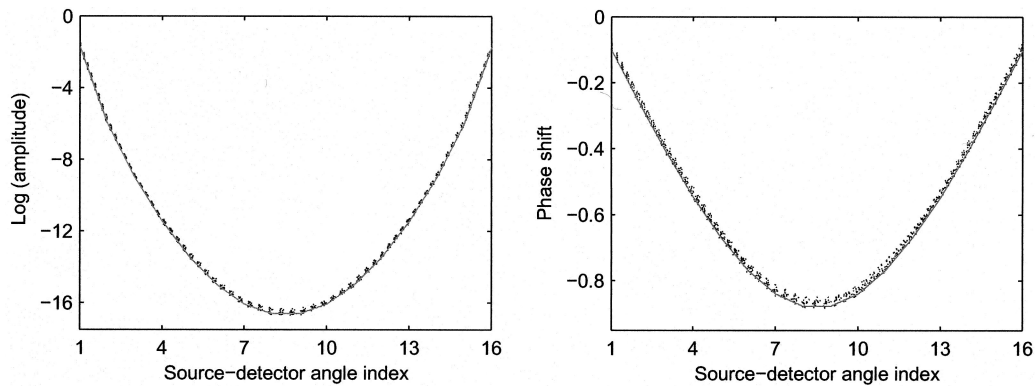


Fig. 1. Left image, logarithm of the amplitude of the simulated data plotted against the source–detector angle index for raw data (dotted curve) and for calibrated data (solid curve). Right image, phase shift of the simulated data plotted against the source–detector angle index for raw data (dotted curve) and for calibrated data (solid curve).

Gaussian-distributed noise with a standard deviation of 1% of corresponding amplitude and phase was added to the simulated data. The amplitude and phase shift of the simulated data are plotted against the source–detector angle index in Fig. 1 as dotted curves.

1. Calibration

The relative source and detector coupling coefficients and transmitted light intensities were solved by minimizing functional (12) with the choice $L = I$.

The minimization problem was solved by Gauss–Newton algorithm (14). The convergence was achieved in three iterations. The relative source and detector amplitude loss coefficients and phase shifts and the corresponding estimated values are shown in Fig. 2. The data was calibrated by use of Eq. (16). The amplitudes and phase shifts of the data against the source–detector angle index before and after calibration are shown in Fig. 1.

The results show that the relative source and detector coupling coefficients can be estimated with

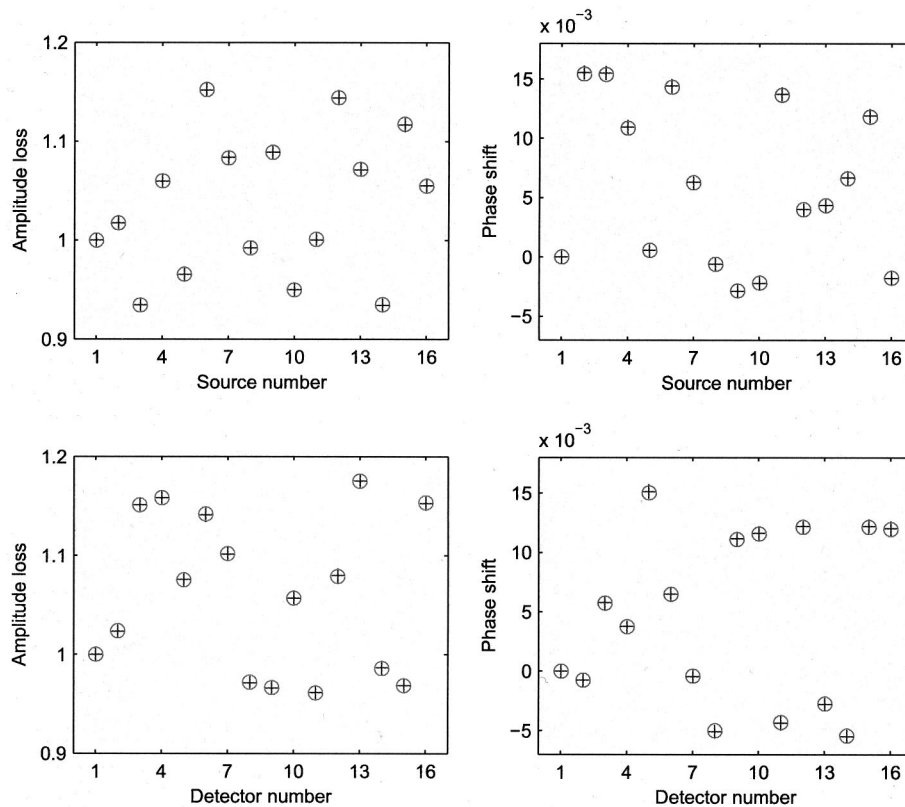


Fig. 2. Top row, relative source amplitude loss coefficient (left image) and phase shift (right image) shown as + and the corresponding estimated values shown as circles. Bottom row, relative detector amplitude loss coefficient (left image) and phase shift (right image) shown as + and the corresponding estimated values shown as circles.

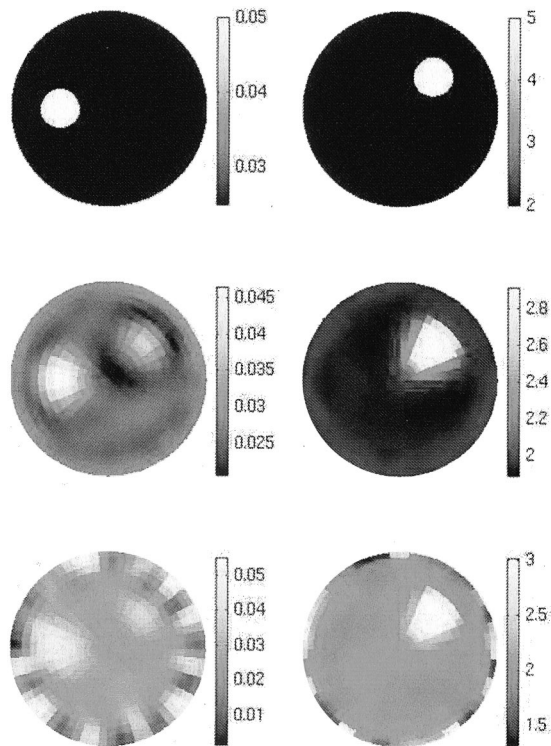


Fig. 3. Absorption coefficients (left column) and scattering coefficients (right column). Top row, simulated distributions; middle row, reconstructions from calibrated data; bottom row, reconstructions from raw data.

good accuracy. The simulated and estimated values are almost equal, which can be seen from Fig. 2. The maximum relative error of the estimated coupling coefficients was approximately 1%. As explained in Section 2, in a rotation symmetric setup the measured amplitudes and phase shifts should be equal with the same source–detector angle index in an ideal case in which there are no source and detector amplitude losses and phase delays. As can be seen from Fig. 1, the calibration compensates for the amplitude losses and phase delays in the data, and thus the calibrated data have much less variation between the sources and the detectors compared with the raw data.

2. Reconstructions

To test the effect of the calibration on the quality of the reconstructed images, other data were generated with the same measurement setup. Now the medium contained two circular inclusions. The absorption and scattering coefficients of the inclusions were $(\mu_a, \mu_s) = (0.05, 2) \text{ mm}^{-1}$ and $(\mu_a, \mu_s) = (0.025, 5) \text{ mm}^{-1}$, respectively. The simulated absorption and scattering distributions are shown in the top row of Fig. 3.

The data were calibrated with Eq. (16) by use of the previously estimated relative coupling coefficients. Then the initial values of the absorption and scatter $(\mu_{a,0}, \mu_{s,0})$, as well as the systematic biases (ξ, ε) in the calibrated data were estimated by minimization of functional (21). In the minimization, the forward

model [Eqs. (17)–(18)] was based on FEM discretization of the “conventional” diffusion approximation; that is, the amplitude loss and phase-shift parameters in Eqs. (34) and (39) were set to values $s_i = d_i = 1, \forall i$ and $\delta_i = \sigma_i = 0, \forall i$, respectively. The weighting matrix L was chosen as in Eq. (13). Functional (21) was minimized by a Gauss–Newton algorithm that was equipped with an explicit line search algorithm for the determination of the step length. Finally, the estimated biases (ξ, ε) were removed from the calibrated data $\hat{\Gamma}$ by Eq. (22), and the absorption and scatter reconstructions were computed with a total variation regularized output least-squares scheme similar to the method described in Ref. 24. The reconstruction mesh contained 496 quadratic reconstruction pixels. The reconstructed absorption and scattering coefficients from the calibrated data and raw data are shown in Fig. 3.

As can be seen from Fig. 3, the calibration improves the quality of the reconstructed images significantly. Although the reconstructions from the raw uncalibrated data are unclear with large perturbations near the boundary, the reconstructions from the calibrated data are clear and the inclusions are well distinguished. Some cross talk between the scattering and the absorption appears in the reconstructions. This, however, is typical for DOT reconstructions.

B. Measurement Results

Measurements were performed with the multichannel optoelectronic near-infrared system for time-resolved image reconstruction (MONSTIR) imaging system of the Biomedical Optics Research Laboratory at University College London. A detailed description of the system and the data-acquisition protocol can be found in Ref. 12.

Measurements with a homogeneous cylindrical phantom were performed to obtain the data for the calibration. The height of the phantom was 14 cm, and the diameter was 7 cm. The absorption coefficient of the phantom was approximately $\mu_a = 0.01 \text{ mm}^{-1}$, and the (reduced) scattering coefficient was approximately $\mu'_s = 1 \text{ mm}^{-1}$. The refractive index was $n_{\text{in}} = 1.56$. A plastic ring was used to hold the 16 sources and 16 detectors in contact with the phantom. A data-acquisition protocol, which ensured that the photon current did not exceed the maximum value allowed in each channel, was performed. Therefore measurements were not made on the detectors closest to each source. The frequency-domain data were obtained by Fourier transforming the measured time-domain data. Data corresponding to the input signal modulation frequency $f = 100 \text{ MHz}$ were chosen. The amplitude and phase shift of the measured data are plotted against the source–detector angle index in Fig. 4 as dotted curves.

1. Calibration

The relative source and detector coupling coefficients and transmitted light intensities were estimated by minimizing functional (12) with the

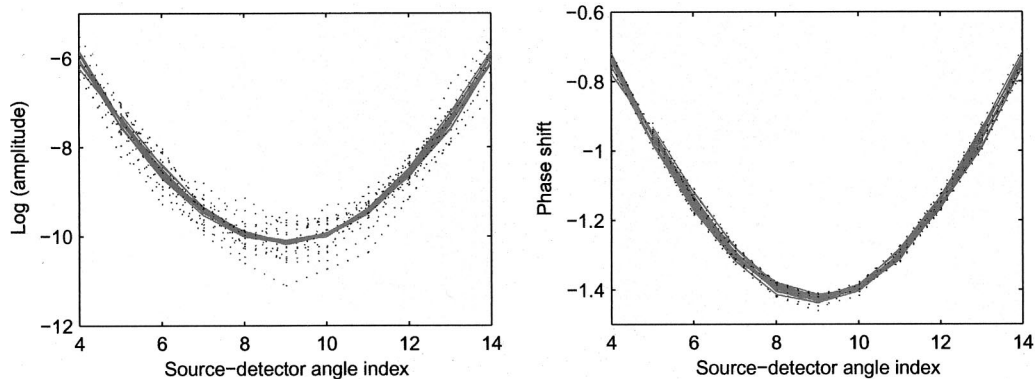


Fig. 4. Left image, logarithm of the amplitude of the measured data plotted against the source–detector angle index for raw data (dotted curves) and for calibrated data (solid curves). Right image, phase shift of the measured data plotted against the source–detector angle index for raw data (dotted curves) and for calibrated data (solid curves).

weighting matrix L as in Eq. (13). The minimization problem was solved by Levenberg–Marquardt algorithm (15) with the stabilization parameter $\lambda = 0.001$. The convergence was achieved in three iterations. The measured data were calibrated with Eq. (16) by means of the estimated coupling coefficients. The amplitudes and phase shifts of the measured data plotted against the source–detector angle index for the raw data and calibrated data are shown in Fig. 4.

A clear difference in variation of the amplitudes of raw and calibrated data can be seen. This indicates that the calibration is correcting for the amplitude losses of the sources and detectors. On the other hand, the calibration does not seem to have a significant effect on the phase shifts. We expect that this is because the phase shifts of the sources and detectors are already efficiently treated by the data-acquisition protocol of the MONSTIR system, and therefore the quality of the phase data is already good.

2. Reconstructions

The effect of calibration on the quality of the reconstructed images was investigated. Therefore another measurement was carried out with the same measurement setup. Two small cylinders were placed inside the phantom. The absorption and scattering coefficients of the cylinders were (approximately) $(\mu_a, \mu'_s) = (0.05, 1) \text{ mm}^{-1}$ and $(\mu_a, \mu'_s) = (0.01, 5) \text{ mm}^{-1}$, respectively. The cylinders were located at the same height as the plastic ring that was holding the source and detector fibers. The measurements were carried out similarly as those for the homogeneous phantom. The measured data were calibrated with Eq. (16) by use of the relative coupling coefficients estimated above, and then we performed the initialization explained in Section 2. Finally, the estimated biases (ξ, ε) were removed from the calibrated data $\tilde{\Gamma}$ by Eq. (22), and the three-dimensional reconstructions were carried out with the frequency-domain version of TOAST (time-resolved optical absorption and scattering tomography) software of the Biomedical Optics Research Laboratory at University College London.²⁵ Three types of images were

reconstructed: a difference image, an absolute image from calibrated data, and an absolute image from raw (uncalibrated) data. The difference image was obtained by use of the data from the homogeneous phantom as reference data and by addition of the calculated difference to the reference values.

The reconstructed absorption and scattering coefficients on the horizontal layer in which the sources and detectors were located are shown in Fig. 5. The absolute reconstructions from the raw data contain severe perturbations near the boundaries of the domain, and the locations of the inclusions are not well distinguished. The absolute images from the cali-

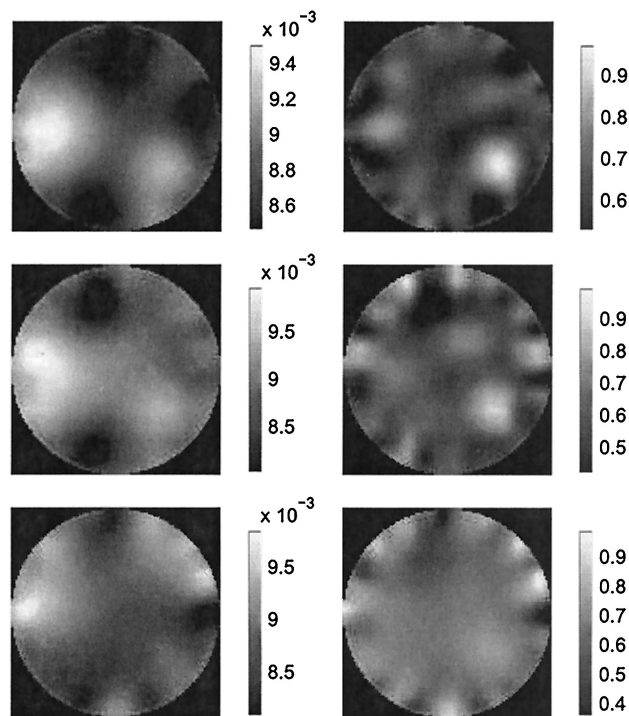


Fig. 5. Absorption coefficients (left column) and scattering coefficients (right column). Top row, difference images; middle row, absolute images from calibrated data; bottom row, absolute images from raw uncalibrated data.

brated data are better than those from the uncalibrated data. In the former, the inclusions are distinguished more clearly, and the number of reconstruction artifacts has decreased significantly. Thus calibration improves the quality of the absolute images.

5. Conclusions

We proposed a computational calibration method for optical tomography. The model of the calibration scheme is based on rotation symmetry of the source and detector positions in the measurement setup. The relative amplitude losses and phase shifts at the optic fibers are modeled by complex-valued coupling coefficients. The relative coupling coefficients can be estimated when data from a homogeneous and isotropic object are given. Once the relative coupling coefficients have been estimated, any data measured with the same measurement setup can be calibrated.

The method was tested with simulations and measurements. The results show that the calibration method can reduce the effects of unknown amplitude losses and phase delays that occur in source and detector fibers. Thus the method can improve the quality of reconstructed images significantly. Therefore the proposed approach offers a simple and accurate method for calibrating optical tomography measurements.

This work was supported by the National Technology Agency of Finland (contract 40781/00), the Wellcome Trust, and the Academy of Finland (decision numbers 206449 and 203985).

References

1. B. W. Pogue, S. P. Poplack, T. O. McBride, W. A. Wells, K. Sunshine Osterman, U. L. Osterberg, and K. D. Paulsen, "Quantitative hemoglobin tomography with diffuse near-infrared spectroscopy: pilot results in the breast," *Radiology* **218**, 261–266 (2001).
2. J. P. Culver, R. Choe, M. J. Holboke, L. Zubkov, T. Durduran, A. Slemple, V. Ntziachristos, B. Chance, and A. G. Yodanis, "Three-dimensional diffuse optical tomography in the parallel plane transmission geometry: evaluation of a hybrid frequency domain/continuous wave clinical system for breast imaging," *Med. Phys.* **30**, 235–247 (2003).
3. J. C. Hebden, A. Gibson, R. M. Yusof, N. Everdell, E. M. C. Hillman, D. T. Delpy, S. R. Arridge, T. Austin, J. H. Meek, and J. S. Wyatt, "Three-dimensional optical tomography of the premature infant brain," *Phys. Med. Biol.* **47**, 4155–4166 (2002).
4. M. A. Franceschini, V. Toronov, M. E. Filiaci, E. Gratton, and S. Fantini, "On-line optical imaging of the human brain with 160-ms temporal resolution," *Opt. Express* **6**, 49–57 (2000), <http://www.opticsexpress.org>.
5. A. V. Bluestone, G. Abdoulaev, C. H. Schmitz, R. L. Barbour, and A. H. Hielscher, "Three-dimensional optical tomography of hemodynamics in the human head," *Opt. Express* **9**, 272–286 (2001), <http://www.opticsexpress.org>.
6. S. Prince, V. Kolehmainen, J. P. Kaipio, M. A. Franceschini, D. Boas, and S. R. Arridge, "Time-series estimation of biological factors in optical diffusion tomography," *Phys. Med. Biol.* **48**, 1491–1504 (2003).
7. T. Noponen, M. Paloheimo, P. Meriläinen, T. Kajava, K. Kotilahti, I. Nissilä, and T. Katila, "Multi-channel near-infrared spectroscopy on the human forehead during hypo- and hypercapnia," in *Biomedical Topical Meetings on CD-ROM* (Optical Society of America, Washington, D.C., 2004), paper WF8.
8. R. Williams and M. Beck, eds., *Process Tomography, Principles, Techniques and Applications* (Butterworth-Heinemann, Oxford, UK, 1995).
9. E. M. C. Hillman, J. C. Hebden, F. E. W. Schmidt, S. R. Arridge, M. Schweiger, H. Dehghani, and D. T. Delpy, "Calibration techniques and datatype extraction for time-resolved optical tomography," *Rev. Sci. Instrum.* **71**, 3415–3427 (2000).
10. I. Nissilä, K. Kotilahti, K. Fallström, and T. Katila, "Instrumentation for the accurate measurement of phase and amplitude in optical tomography," *Rev. Sci. Instrum.* **73**, 3306–3312 (2002).
11. T. O. McBride, B. W. Pogue, S. Jiang, U. L. Österberg, and K. D. Paulsen, "A parallel-detection frequency-domain near-infrared tomography system for hemoglobin imaging of the breast *in vivo*," *Rev. Sci. Instrum.* **72**, 1817–1824 (2001).
12. F. E. W. Schmidt, M. E. Fry, E. M. C. Hillman, J. C. Hebden, and D. T. Delby, "A 32-channel time-resolved instrument for medical optical tomography," *Rev. Sci. Instrum.* **71**, 256–265 (2000).
13. D. A. Boas, T. Gaudette, and S. R. Arridge, "Simultaneous imaging and optode calibration with diffuse optical tomography," *Opt. Express* **8**, 263–270 (2001), <http://www.opticsexpress.org>.
14. J. J. Stott, J. P. Culver, S. R. Arridge, and D. A. Boas, "Optode positional calibration in diffuse optical tomography," *Appl. Opt.* **42**, 3154–3162 (2003).
15. S. Oh, A. B. Milstein, R. P. Millane, C. A. Bouman, and K. J. Webb, "Source-detector calibration in three-dimensional Bayesian optical diffusion tomography," *J. Opt. Soc. Am. A* **19**, 1983–1993 (2002).
16. T. O. McBride, B. W. Pogue, U. L. Österberg, and K. D. Paulsen, "Strategies for absolute calibration of near infrared tomographic tissue imaging," in *Oxygen Transport to Tissue XXIV*, J. F. Dunn and H. M. Swartz, eds. (Kluwer Academic-Plenum, New York, 2003), pp. 85–99.
17. C. H. Schmitz, H. L. Graber, H. Luo, I. Arif, J. Hira, Y. Pei, A. Bluestone, S. Zhong, R. Andronica, I. Soller, N. Ramirez, S.-L. S. Barbour, and R. L. Barbour, "Instrumentation and calibration protocol for imaging dynamic features in dense-scattering media by optical tomography," *Appl. Opt.* **39**, 6466–6486 (2000).
18. D. W. Marquardt, "An algorithm for least-squares estimation of nonlinear parameters," *J. Soc. Ind. Appl. Math.* **11**, 431–441 (1963).
19. M. Schweiger and S. R. Arridge, "The finite-element method for the propagation of light in scattering media: frequency domain case," *Med. Phys.* **24**, 895–902 (1997).
20. J. Heino and E. Somersalo, "Estimation of optical absorption in anisotropic background," *Inverse Probl.* **18**, 559–573 (2002).
21. M. Schweiger, S. R. Arridge, M. Hiraoka, and D. T. Delpy, "The finite element method for the propagation of light in scattering media: boundary and source conditions," *Med. Phys.* **22**, 1779–1792 (1995).
22. S. R. Arridge, "Optical tomography in medical imaging," *Inverse Probl.* **15**, R41–R93 (1999).
23. S. R. Arridge, M. Schweiger, M. Hiraoka, and D. T. Delpy, "A finite element approach for modeling photon transport in tissue," *Med. Phys.* **20**, 299–309 (1993).
24. V. Kolehmainen, "Novel approaches to image reconstruction in diffusion tomography," Ph.D. thesis (University of Kuopio, Kuopio, Finland, 2001).
25. S. R. Arridge and M. Schweiger, "The UCL optical tomography software system (TOAST)," available at <http://www.medphys.ucl.ac.uk/~martins/toast/index.html>.